Microwave filters based on novel dielectric split-ring resonators with high unloaded quality factors

Noori, Ahmed S.; Shang, Xiaobang; Guo, Cheng; Jackson, Timothy J.; Smith, Paul A.; Lancaster, Michael J.

DOI:
10.1049/iet-map.2017.0463

IET Microwaves, Antennas & Propagation

Research Article

IET Journals
The Institution of Engineering and Technology

Microwave filters based on novel dielectric split-ring resonators with high unloaded quality factors

ISSN 1751-8725
Received on 12th June 2017
Revised 4th November 2017
Accepted on 16th February 2018
doi: 10.1049/iet-map.2017.0463
www.ietdl.org

Ahmed S. Noori[1] ✉, Xiaobang Shang[1], Cheng Guo[1], Timothy J. Jackson[1], Paul A. Smith[1], Michael J. Lancaster[1]

[1]*School of Electrical, Electronic and Systems Engineering, University of Birmingham, Edgbaston, Birmingham B15 2TT, UK*
✉ *E-mail: asabah22@gmail.com*

Abstract: Here, the authors present a new type of split-ring resonator (SRR) constructed from high dielectric constant material. Compared to conventional metal SRRs, such resonators have significantly higher unloaded quality factor (Q_u). A new class of microwave filter is presented using the dielectric SRR. Two examples of different filter configurations are investigated, and the measured results show excellent performance. Good agreement between measurements and simulations has been achieved.

1 Introduction

Filters formed of resonators with high unloaded quality factor (Q_u) are in demand for applications with stringent requirements on insertion loss, this includes satellite systems and wireless base stations [1–4] as well as many others. Dielectric resonators (DRs) are a popular choice for such applications [1–8]. Another common high Q_u resonator is the metal or less common dielectric combline resonator, the latter has a Q_u as high as DRs (≃10,000 at S band and $\varepsilon_r = 36$) [1, 9]. The electromagnetic field distributions and filter configuration for this dielectric combline is approximately the same as the conventional metal combline resonator, provided the dielectric constant is high [9–12].

Another type of resonator is the metal split-ring resonator (SRR) with Q_u of ∼4000 at S band manufactured with copper material [13–15]. This resonator is a hollow cylindrical ring with a longitudinal gap as shown in Fig. 1. Cavity filters based on metal-SRR are rarely reported [13, 14], but the metal-SRRs used more with the microwave sensors [16–21].

This paper investigates an SRR but with the metal replaced by a high permittivity dielectric. Such dielectric-SRRs have similar electromagnetic field distributions as the metal-SRR, but importantly, they have a higher Q_u if made of a low-loss dielectric material. The higher Q_u is due to the removal of the conduction current on the surface of the metal-SSR where most of the losses conventionally occur. As these ohmic losses are removed, the main contribution to the loss in the dielectric-SRR is loss tangent of the dielectric material forming the resonator [9, 22].

The Q_u of the dielectric-SRR can be even higher than the Q_u of DRs with the same ε_r and loss tangent. This is because with DRs, most of the energy is stored inside the DR [1, 22] which presents losses due to the loss tangent of dielectric material. In the case of dielectric-SRR, most of the energy is stored outside the dielectric material which reduces the effect of the loss tangent.

This paper looks at filters where the dielectric-SSRs are all in the same plane, alternatives have been investigated for metal-SRRs where they are placed on the top of each other in a cylindrical housing [13, 14]. The advantage of a planer configuration is it can easily achieve only electric or magnetic coupling between two adjacent resonators. Here, full-wave analysis software (CST [23]) and the methodology of coupled resonator circuits [24] have been used to design new class of filter with examples of two high Q_u filters based on the novel dielectric-SRRs.

Fig. 1 *Metal split-ring resonator (metal-SRR)*

2 Dielectric-SRR

The dielectric-SRR and metal-SRR have been modelled with the same dimensions as shown in Fig. 2*a*. Each is mounted on Teflon holder and in a copper enclosure, as shown in Fig. 2*b*. The fundamental mode field distributions have been simulated using an Eigenmode solver, and the results are shown in Fig. 3. As expected, most electric field is in the gap and the magnetic field peaks at the opposite side of the loop in both metal and dielectric SSRs. The fields are not high inside the dielectric material of the dielectric-SRR.

The dielectric and metal SSR have also been made, and the measurements together with the simulation results and are summarised in Table 1 which include details of the loss tangent for the high dielectric constant materials. It can be seen in Table 1 that the dielectric-SRR has a Q_u around three times higher than that of metal-SRR in exactly the same configuration. Note the metal-SSR has a slightly lower frequency than the dielectric-SSR. However, simulations show that if the metal-SSR is reduced in size to give the same frequency as the dielectric-SSR (2.3 GHz) then the Q_u changes to 6200 still almost three times lower than the dielectric-SSR.

The Q_u of the dielectric-SRR shown in Fig. 2 is now compared with Q_u of the disk/cylindrical DR at fundamental resonance frequency of 2.3 GHz with the same ε_r and loss tangent. The DR model is shown in Fig. 4, with the ratio of $W/2R = 0.4$ to achieve the best Q_u for the fundamental mode [1]. It is mounted on a Teflon holder and in a copper enclosure of 30 mm diameter and 50 mm height. Table 2 shows the CST Eigenmode simulation results for comparison between the now named dielectric-SRR1 and the DR1.

The comparison in Table 2 shows that for this particular configuration, the Q_u of the dielectric-SRR1 is 50% higher than the Q_u of DR1, but the radius of the dielectric-SRR1 is about twice that of the radius of DR1. It is the high Q_u which is of interest here and the fact that they are slightly larger than DR is of less importance.

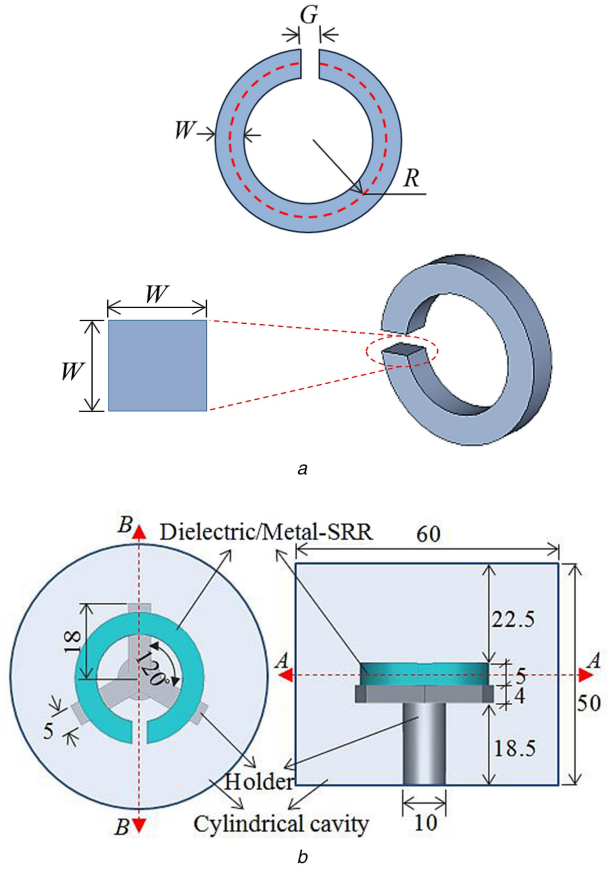

Fig. 2 *Configuration and dimensions in (mm)*
(a) Dielectric/metal-SRR: $G = 3.5$, $R = 12.5$, and $W = 5$, ***(b)*** Single resonator inside metal enclosure and mounted on PTFE holder

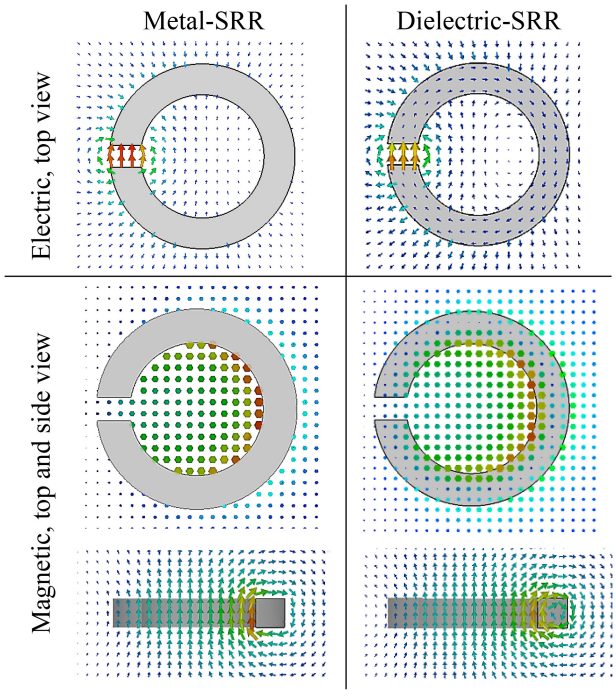

Fig. 3 *Electromagnetic field distributions for dielectric-SRR of $\varepsilon_r = 97$ and metal-SRR. Section AA for top view and BB for side view, see Fig. 2b*

There are other advantages of the SRR not used in the filters in this paper, this includes the ability to produce tuneable coupling by just rotation of the resonators [25] and the electromagnetic field distributions are very useful for the microwave sensors [16–21].

The dielectric constant (ε_r) of the material making the SSRs and DRs influences the amount of stored energy inside resonators. For instance, dielectric material of $\varepsilon_r = 97$ stores more energy inside the resonator than the case when $\varepsilon_r = 36$ [1, 6]. For this reason, the comparison between dielectric-SRR1 and DR1 has been repeated with the same enclosure and both resonators having the commonly used ε_r of 36. This is shown in Table 3. The Eigenmode CST simulation results in Table 3 have revealed the dielectric-SRR2 has a Q_u higher than DR2 by 30%. This percentage increase is less than the percentage increase from the comparison in Table 2, but is still significant. Again the dielectric-SRR2 has radius about twice the radius of DR2.

The dielectric-SSR configuration in Fig. 2 has been used to find the effects of dimensions on the fundamental mode frequency with the results shown in Fig. 5. These were all simulated with $\varepsilon_r = 97$. The gap of dielectric-SRR can be considered to represent a capacitor and loop represents inductor in the resonator equivalent

Table 1 Q_u comparison for dielectric-SRR and metal-SRR. Both resonators have same dimensions as in Fig. 2

	Dielectric-SRR Titania, $\varepsilon_r = 97$ Tan $\delta = 7.2 \times 10^{-5}$ at (2.3 GHz)		Metal-SRR copper $\sigma = 5.813 \times 10^7$	
	Simulated	Meas.	Simulated	Meas.
f, GHz	2.3	2.29	1.66	1.68
Q_c cavity	122,510	—	124,010	—
Q_c resonator	—	—	7,176	—
Q_d holder	315,080	—	108,810	—
Q_d resonator	24,502	—	—	—
Q_u	19,176	17,021	6,732	4,630

Q_c, conductive quality factor; Q_d, dielectric quality factor.

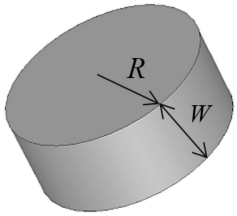

Fig. 4 *Configuration of disk DR. R is the radius and W is the height of DR*

Table 2 Eigenmode CST simulation results for comparison between dielectric-SRR1 and DR1

	Titania, $\varepsilon_r = 97$ tan $\delta = 7.2 \times 10^{-5}$ at 2.3 GHz	
	Dielectric-SRR1	DR1
resonator size, mm	$G = 3.5$, $R = 12.5$, $W = 5$	$R = 7.5$, $W = 6$
f	2.3 GHz	2.3 GHz
Q_c	122,510	112,890
Q_d	22,734	14,030
Q_u	19,176	12,478

Table 3 Eigenmode CST simulation results for comparison between dielectric-SRR2 and DR2

	$\varepsilon_r = 36$, tan $\delta = 1 \times 10^{-4}$ at 4.5 GHz	Material series 8300 from trans-tech manufacture [1]
	Dielectric-SRR2	DR2
resonator size, mm	$G = 1$, $R = 12.5$, $W = 5$	$R = 6$, $W = 5$
f	4.5 GHz	4.5 GHz
Q_c	61,696	116,810
Q_d	15,748	10,228
Q_u	12,546	9,404

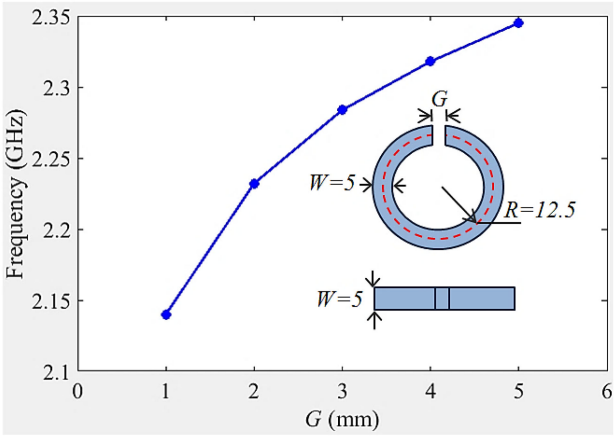

a

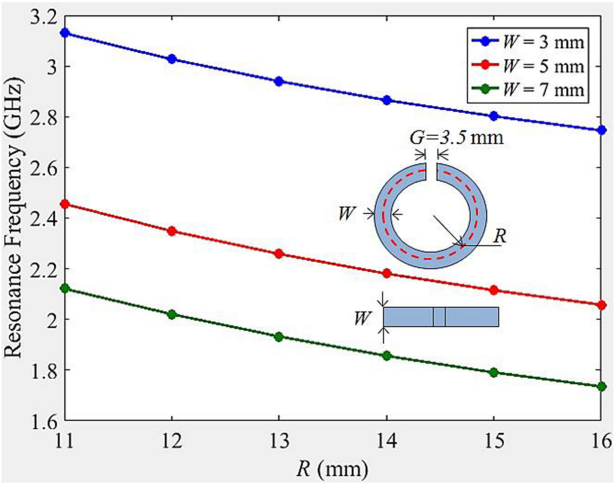

b

Fig. 5 *Fundamental resonance frequency f against dielectric-SRR dimensions*
(a) *f* against *G*, ***(b)*** *f* against *R* and *W*

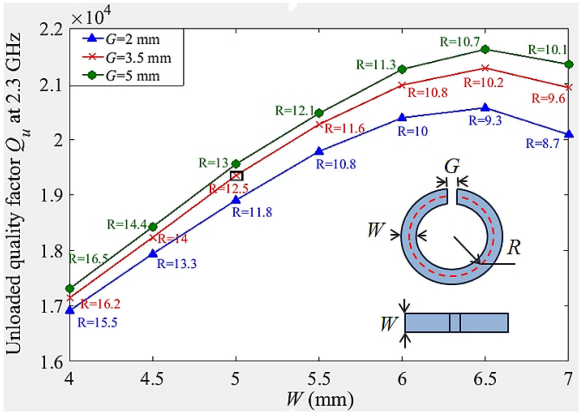

Fig. 6 *Q_u against dielectric-SRR dimensions. The point inside a square indicates to dielectric-SRR dimensions (G = 3.5, R = 12.5, and W = 5 mm) has chosen in this paper*

circuit. Increasing the gap (G) (when the radius (R) and cross-section (W) are fixed) decreases the capacitance leading to an increase in the resonance frequency in Fig. 5*a*. The resonance frequency decreases when R increases due to an increase in the inductance loop length (Fig. 5*b*). The cross-section (kept square in this case) has more effect on the resonance frequency than G and R because increasing W will increase the capacitor surface area, leading to a decrease in the resonance frequency as shown in Fig. 5*b*.

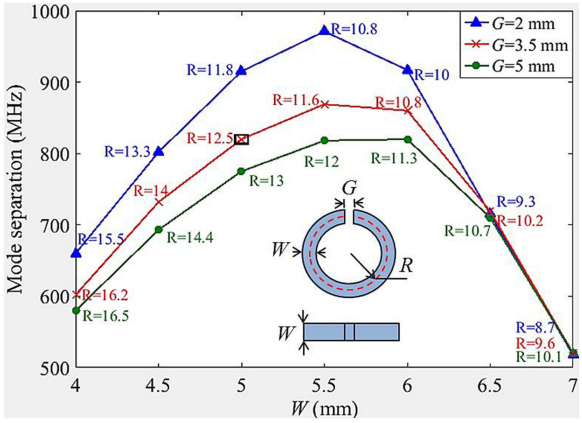

Fig. 7 *Mode separation against dielectric-SRR dimensions. The point inside a square indicates the dielectric-SRR dimensions (G = 3.5, R = 12.5, and W = 5) chosen as an example in this paper*

The effects of dielectric-SRR dimensions, with $\varepsilon_r = 97$ and loss tangent of 7.2×10^{-5}, on the Q_u at the fundamental mode of 2.3 GHz are shown in Fig. 6. The same model shown in Fig. 2 is used in the Eigenmode simulation. The metal enclosure radius is kept to twice the dielectric-SRR radius (R) even when varying the R to decrease the enclosure effect on Q_u. The conductive quality factors due to the walls, Q_c, for all results in Fig. 6 are from 122,700 to 124,500, showing the walls have a minimal effect on the total Q_u. Here, W is varied with three different G values; with R tuned to fix the fundamental mode at 2.3 GHz. W has significant effect on Q_u due to increased gap area of the dielectric-SRR and the overall volume of resonator.

The mode separation between the fundamental mode of 2.3 GHz, and the first higher-order mode against dielectric-SRR dimensions, are shown in Fig. 7. The simulation results show the best mode separation can be achieved when W is from ~5 to 6 mm depending upon the value of G.

3 Filter design

In order to design filters using the coupled resonator approach [24], we need to consider both the coupling to an external input/output transmission line and the coupling between two resonators. This is done in the following two sections followed by the full filter design.

3.1 Coupling between resonators

The dielectric-SRRs ($\varepsilon_r = 97$) with dimensions as shown in Fig. 2*a* and holder with $\varepsilon_r = 2.1$ with dimensions as shown in Fig. 2*b* have been chosen for the filter design. Firstly, we need to extract the coupling coefficients between two adjacent dielectric-SRRs. The published work about metal-SRR filters considered only a coaxial configuration [13, 14]. In this paper, novel dielectric-SRRs with a planer configuration have been examined. This introduces more flexibility in the design and can easily achieve electric coupling as well as magnetic and mixed coupling.

The coupling coefficients (K_c) are extracted by CST software for configuration when the angle θ_1 of the first resonator and the angle θ_2 of the second resonator are 90°, as shown in Fig. 8*a*. On the dimensional scales shown, the K_c values are small and nearly independent of the distance S between resonators. This is due to both electric and magnetic couplings providing partial cancellation and the coupling can be increased by having a metal wall between dielectric-SRRs. This is only from one side as shown by the inset in Fig. 8*b*. The K_c for configuration in Fig. 8*b* can be controlled by varying the metal wall dimensions between dielectric-SRRs as well as the distance S.

Alternatively, significant, usable values for K_c can be obtained, without the metal wall, by changing the dielectric-SRRs angles (θ_1 and θ_2) and varying distance S as shown in Fig. 9. A further

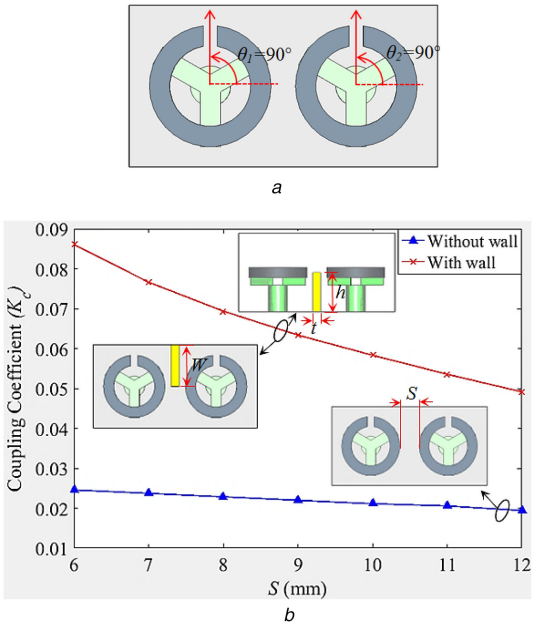

Fig. 8 *Two dielectric-SRRs inside metal enclosure*
(a) Top view with angle θ_1 and $\theta_2 = 90°$, ***(b)*** K_c against distance S with and without wall. Wall dimensions: $W = 20$, $h = 20$, and $t = 4$ mm

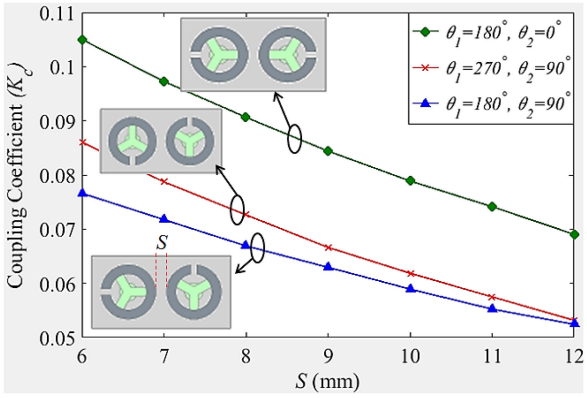

Fig. 9 *K_c of two dielectric-SRRs against distance S for different angles*

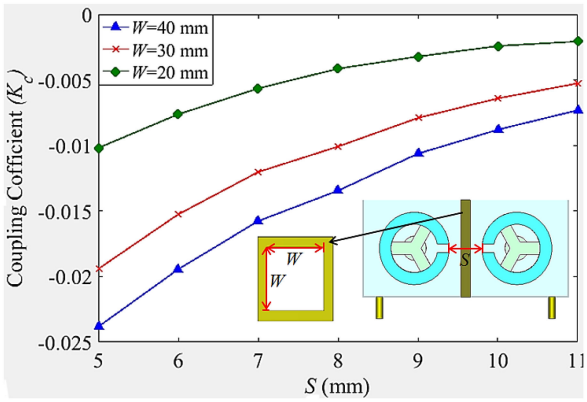

Fig. 10 *Electric K_c of two dielectric-SRRs against distance S and aperture W*

configuration is shown in Fig. 10, when the gaps of two adjacent dielectric-SRRs face each other with a wall coming down from the top of the cavity housing in this case. This configuration can easily achieve electric coupling with the negative K_c values as given in Fig. 10. It should be noted there are many more possibilities for coupling the resonators, for example, as a function of the rotation angle θ. However, only the coupling used in the filters have been discussed here.

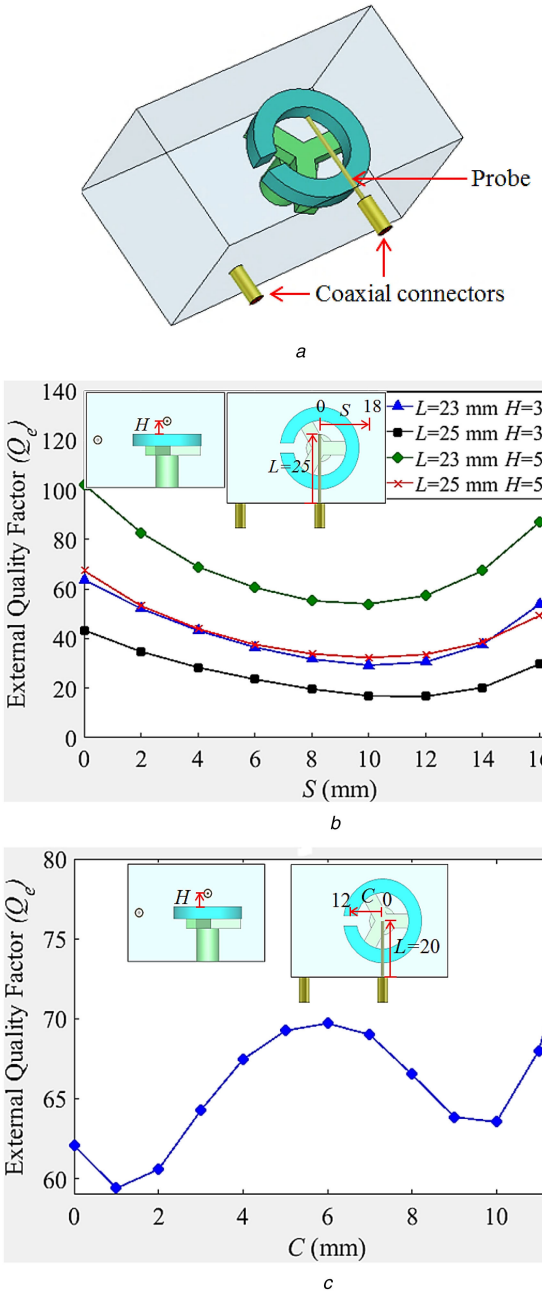

Fig. 11 *Simulation model and results of Q_e*
(a) Single dielectric-SRR inside metal enclosure, ***(b)*** Q_e of the probe has moved from resonator centre to its loop, with different lengths (L) and heights (H), ***(c)*** Q_e of the probe has moved from resonator centre to its gap with $H = 1$ mm

3.2 Extraction of external quality factor

The coupling to the input and output, as defined though the external quality factor Q_e, for the dielectric-SRRs is extracted based on the method described in [24]. This coupling is achieved through a probe as shown in Fig. 11*a*. The model configuration and CST simulation results for Q_e against two different probe lengths (L) and heights (H) for probe moving from the centre of dielectric-SRR towards right are shown in Fig. 11*b*.

In addition, the Q_e is extracted when moving the feeding probe from dielectric-SRR centre towards the left where the gap is located. This is shown in Fig. 11*c*. There are many other possibilities of coupling to the resonator, such as the rotation angle of the resonator or the probe vertical position, but we limit the discussion to this particular structure which has been found suitable for the filters described below.

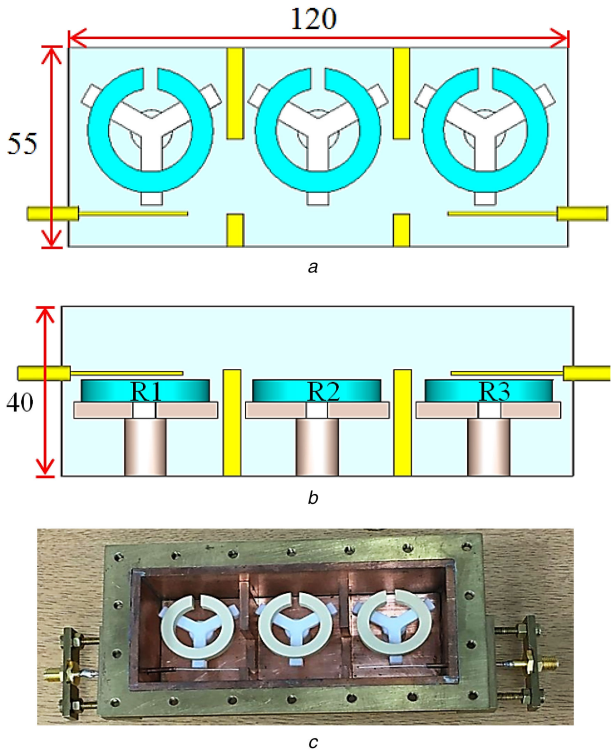

Fig. 12 *Third-order dielectric-SRR filter configuration*
(a) Top view, ***(b)*** Side view. R1, 2, and 3 indicate to resonators, ***(c)*** Fabricated filter with lid removed. Unit: millimetre

3.3 Third-order filter

This filter is designed to have a Chebyshev response, with a centre frequency of 2.2 GHz, fractional bandwidth (FBW) of 5%, and return loss of 20 dB. The non-zero coupling coefficients of filter are calculated to be $M_{12} = M_{23} = 0.05$, and the external quality factor are $Q_{e1} = Q_{e2} = 17$ [24]. Fig. 12 shows the filter configuration as well as overall dimensions and the fabricated filter. Detailed dimensions of the resonators and holders can be found in Fig. 2.

The simulation and measurement results are shown in Fig. 13*a*. The S_{21} response is not symmetrical; this is due to the appearance of a transmission zero. Simulation has shown this zero is attributed to the unwanted cross-coupling between the input and output coaxial cables. Such a transmission can be moved in frequency or suppressed by a more complex use of walls. However, this study is not part of this work. There is a small frequency shift in measured response, and this is due to small errors in fabrication. Note that there has been no tuning of the filter. Tuning screws are able to correct this small frequency shift; however, the agreement is good and therefore, we have not done the tuning. Results without tuning demonstrate more about the accurate construction and design than do tuned results.

The return loss is >20 dB which is an excellent result. The measured insertion loss is ~0.3 dB higher than simulated. From this measured insertion loss, the effective unloaded Q of resonators can be calculated as 11,125 [24]. This can be compared with 19,176 in Table 2. So both the insertion loss and Q_u tell us that are additional unexpected losses. This can be attributed to (i) potential small errors in the assumed material parameters such as the loss tangent, (ii) the losses in the 3 cm semi-rigid cables connecting to the devices, (iii) losses in SMA connectors, (iv) manufacturing problems, particularly with the cables and earth connection to the outer cavity, and (v) the small effect of the return loss on the insertion loss. Some of these errors are small, some are difficult to quantify, but the expectation is that the additional loss is a combination.

The S_{21} responses across a wider band are shown in Fig. 13*b*, the first higher spurious response occurs at 2.85 GHz, and is at a similar frequency to simulation results of the single dielectric-SRR and comparable with the spurious performance of DR filters [1].

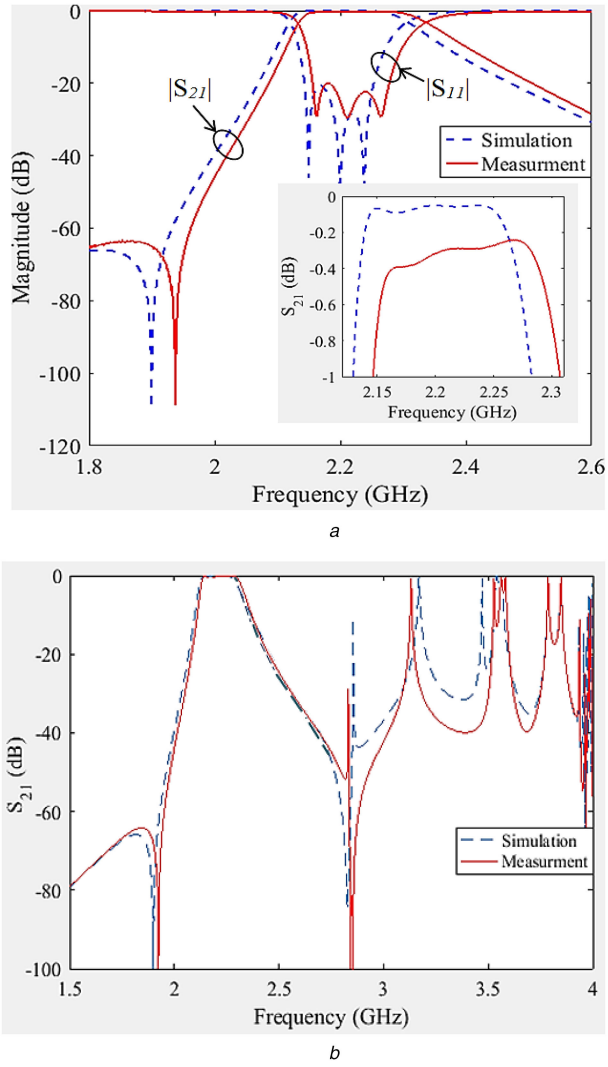

Fig. 13 *Measured and simulated responses of the third-order dielectric-SRR filter*
(a) Close to the centre frequency, ***(b)*** Wider band showing the spurious response

3.4 Fourth-order filter with symmetric transmission zeros

This filter is designed to have a centre frequency of 2.3 GHz, FBW of 4%, and return loss of 20 dB. A cross-coupling is added between resonators R1 and R4 to provide a pair of transmission zeros at the frequencies of 2.227 and 2.374 GHz. The non-zero coupling coefficients are calculated as [24] $M_{12} = M_{24} = 0.033$, $M_{23} = 0.032$, and $M_{14} = -0.01$, and the external quality factor are $Q_{e1} = Q_{e2} = 24$. The configuration and filter dimensions as well as the fabricated filter are shown in Fig. 14, the dimensions of the resonator and holder as given in the previous section in Fig. 2. Note that between resonators R1 and R4, there is the negative electric coupling required to generate the transmission zeros as discussed previously and shown in Fig. 14.

The simulation and measurement results are shown in Fig. 15. Again this filter has an excellent return loss of >20 dB with a minimum insertion loss of only ~0.3 dB. The untuned filter has a small frequency shift which also moves the position of the transmission zeros slightly.

4 Conclusion

A new high Q_u resonator has been described; it uses a high dielectric constant material to implement a dielectric-SRR, rather than the conventional metal-SRR. The novel dielectric-SRR has higher Q_u than both the metal-SRR and the conventional disk DR.

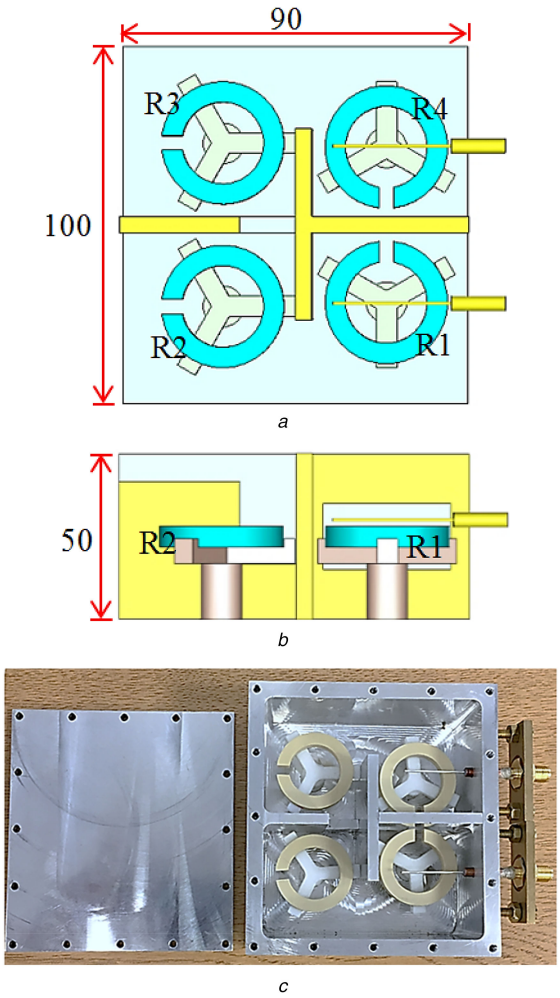

Fig. 14 *Fourth-order dielectric-SRR filter configuration*
(a) Top view, ***(b)*** Side view, R1, 2, and 3 indicate to resonators, ***(c)*** Fabricated filter. Unit: millimetre

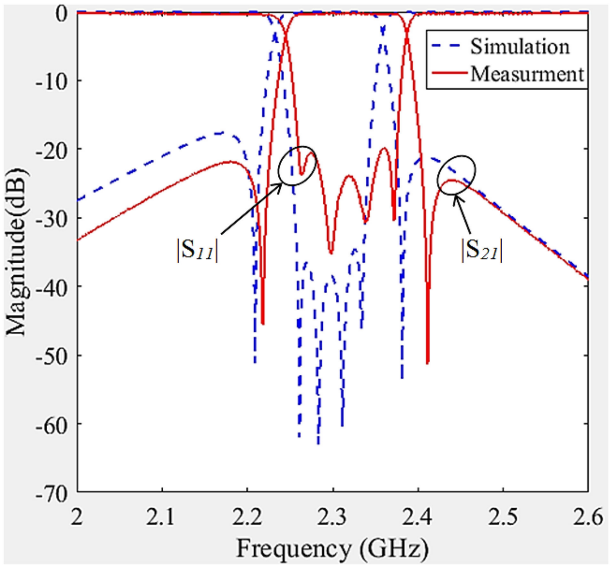

Fig. 15 *Measurement and simulation results of the fourth-order dielectric-SRR filter*

The effect of dielectric-SRR dimensions on the Q_u and mode separation has been described.

For filter design, the internal and external couplings for dielectric-SRRs have been extracted and studied. A new class of microwave filter have been presented with third- and fourth-order examples based on the novel dielectric-SRRs and the method of a coupled resonator circuits. The measurement results of both filters have very good agreement with the simulation results and a very low insertion loss, of ~0.3 dB, has been achieved.

5 Acknowledgments

Ahmed S. Noori would like to thank the Iraqi Ministry of Higher Education and Scientific Research and Wasit University for financing his PhD study at the University of Birmingham. The work has been partly funded by the UK Engineering and Physical Science Research Council.

6 References

[1] Wang, C., Zaki, K.A.: 'Dielectric resonators and filters', *IEEE Microw. Mag.*, 2007, **8**, (5), pp. 115–127
[2] Mansour, R.R.: 'Filter technologies for wireless base stations', *IEEE Microw. Mag.*, 2004, **5**, (1), pp. 68–74
[3] Cameron, R.J.: 'Advanced coupling matrix synthesis techniques for microwave filters', *IEEE Microw. Theory Tech., Trans.*, 2003, **51**, pp. 1–10
[4] Zhang, D.-D., Zhou, L., Wu, L.-S., *et al.*: 'Novel bandpass filters by using cavity-loaded dielectric resonators in a substrate integrated waveguide', *IEEE Trans. Microw. Theory Tech.*, 2014, **62**, (5), pp. 1173–1182
[5] Penaranda-Foix, F.L., Janezic, M.D., Catala-Civera, J.M., *et al.*: 'Full-wave analysis of dielectric-loaded cylindrical waveguides and cavities using a new four-port ring network', *IEEE Trans. Microw. Theory Tech.*, 2012, **60**, (9), pp. 2730–2740
[6] Mansour, R.R., Huang, F., Fouladi, S., *et al.*: 'High-Q tunable filters: challenges and potential', *IEEE Microw. Mag.*, 2014, **15**, (5), pp. 70–82
[7] Chu, Q.X., Ouyang, X., Wang, H., *et al.*: 'TE$_{01\delta}$-mode dielectric-resonator filters with controllable transmission zeros', *IEEE Trans. Microw. Theory Tech.*, 2013, **61**, (3), pp. 1086–1094
[8] Fiedziuszko, S.J., Hunter, I.C., Itoh, T., *et al.*: 'Dielectric materials, devices, and circuits', *IEEE Trans. Microw. Theory Tech.*, 2002, **50**, (3), pp. 706–720
[9] Wang, C., Zaki, K.A., Atia, A.E., *et al.*: 'Dielectric combline resonators and filters', *IEEE Trans. Microw. Theory Tech.*, 1998, **46**, pp. 2501–2506
[10] Mansour, R.R.: 'High-Q tunable dielectric resonator filters', *IEEE Microw. Mag.*, 2009, **10**, (6), pp. 84–98
[11] Zhan, Y., Chen, J.X., Qin, W., *et al.*: 'Spurious-free differential bandpass filter using hybrid dielectric and coaxial resonators', *IEEE Microw. Wirel. Compon. Lett.*, 2016, **26**, (8), pp. 574–576
[12] Kajfez, D., Guillon, P.: '*Dielectric resonators*' (Noble, Atlanta, GA, 1998, 2nd edn.)
[13] Mehdizadeh, M., Ishi, T.K., Hyde, J.S., *et al.*: 'Loop-gap resonator: a lumped mode microwave resonant structure', *IEEE Trans. Microw. Theory Tech.*, 1983, **MTT-31**, pp. 1059–1063
[14] Mostafavi, R.F., Mirshekar-Syahkal, D., Lim, Y.C.: 'Small filters based on slotted cylindrical-ring resonators', *IEEE Trans. Microw. Theory Tech.*, 2001, **49**, pp. 2369–2375
[15] Salehi, H., Mansour, R.R., Dokas, V.: 'Lumped-element conductor-loaded cavity resonators', *IEEE MTT-S Int. Microw. Symp. Dig.*, 2002, **3**, pp. 1601–1604
[16] Bobowski, J.S.: 'Using split-ring resonators to measure the electromagnetic properties of materials: an experiment for senior physics undergraduates', *Am. J. Phys.*, 2013, **81**, (12), pp. 899–906
[17] Choi, H., Naylon, J., Luzio, S., *et al.*: 'Design and in vitro interference test of microwave noninvasive blood glucose monitoring sensor', *IEEE Trans. Microw. Theory Tech.*, 2015, **63**, (10), pp. 3016–3024
[18] Rowe, D.J., Al-Malki, S., Abduljabar, A.A., *et al.*: 'Improved split-ring resonator for microfluidic sensing', *IEEE Trans. Microw. Theory Techn.*, 2014, **62**, (3), pp. 689–699
[19] Masood, A., Castell, O., Barrow, D.A., *et al.*: 'Split ring resonator technique for compositional analysis of solvents in microcapillary systems'. Proc. Int. Conf. MicroTAS, San Diego, USA, October 2008, pp. 1636–1638
[20] Violetti, M., Pellaton, M., Merli, F., *et al.*: 'The microloop-gap resonator: a novel miniaturized microwave cavity for double-resonance rubidium atomic clocks', *IEEE J. Sensors*, 2014, **14**, (9), pp. 3193–3200
[21] Sakamoto, Y., Hirata, H., Ono, M.: 'Design of a multicoupled loop-gap resonator used for pulsed electron paramagnetic resonance measurements', *IEEE Trans. Microw. Theory Tech.*, 1995, **MTT-43**, pp. 1840–1847
[22] Pozar, D.: '*Microwave engineering*' (John Wiley & Sons, Inc., 2012, 4th edn.)
[23] CST Computer Simulation Technology AG., USA (July 2015). [Online]. Available at www.cst.com
[24] Hong, J.-S., Lancaster, M.J.: '*Microstrip filters for RF/microwave applications*' (John Wiley & Sons, Inc., 2001)
[25] Sun, H., Wen, G., Huang, Y., *et al.*: 'Tunable band notch filters by manipulating couplings of split ring resonators', *Appl. Opt.*, 2013, **52**, pp. 7517–7522